

The Cross Equatorial Transport of the Hunga Tonga-Hunga Ha’apai Eruption Plume

Mark Schoeberl¹, Yi Wang¹, Rei Ueyama², Ghassan Taha³, and Wandu Yu⁴

¹Science and Technology Corporation

²NASA Ames Research Center

³Morgan State University

⁴Hampton University

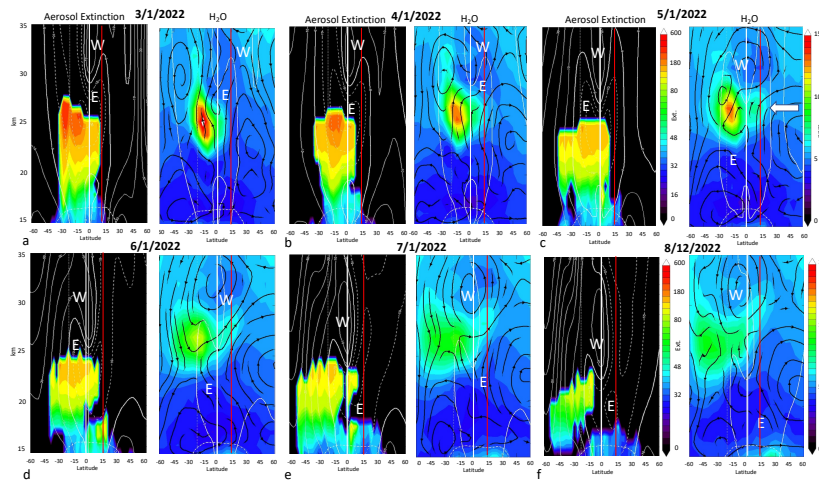
January 3, 2023

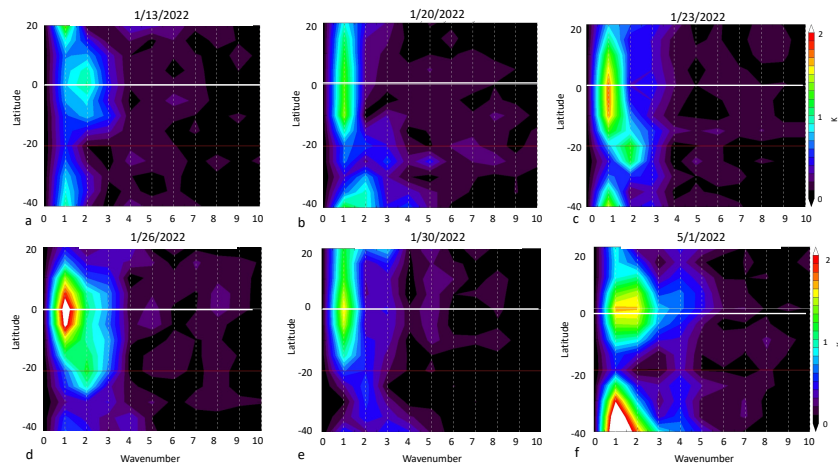
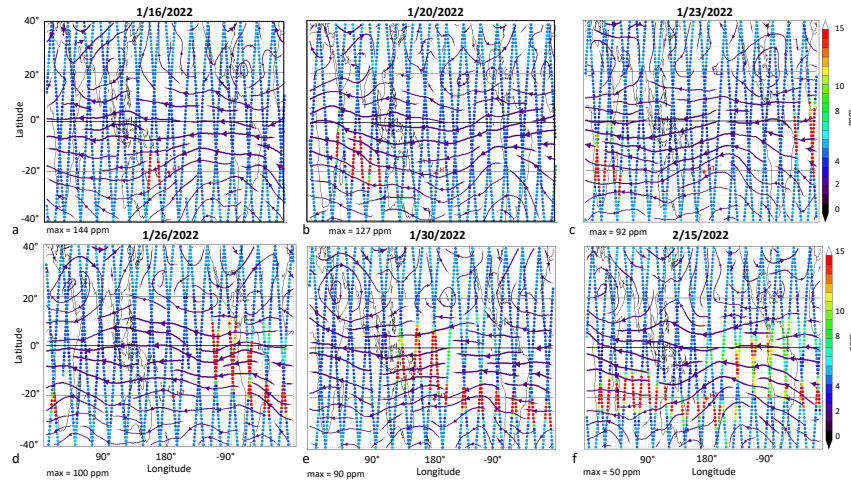
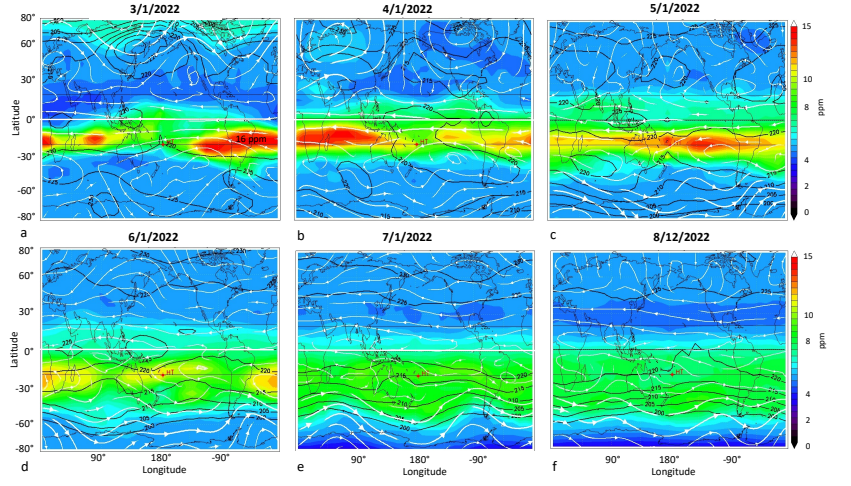
Abstract

On Jan. 15, 2022, the Hunga Tonga-Hunga Ha’apai (HT) eruption injected SO₂ and water into the middle stratosphere. Shortly after the eruption, the water vapor anomaly moved northward toward and across the equator. This northward movement appears to be due to a Rossby wave forced by the excessive IR water vapor cooling. Following the early eruption stage, persistent mid-stratospheric water vapor and aerosol layers were mostly confined to Southern Hemisphere (SH) tropics (Eq. to 30°S). However, during the spring of 2022, the westerly phase of the tropical quasi-biennial oscillation (QBO) descended through the tropics. The HT water vapor and aerosol anomalies were observed to again split across the equator coincident with the descent of the QBO shear zone. This split occurred because of the enhanced meridional transport circulation associated with the QBO. Neither transport event can be reproduced using MERRA2 assimilated winds.

Hosted file

951584_0_art_file_10512913_rmhss6.docx available at <https://authorea.com/users/523044/articles/611246-the-cross-equatorial-transport-of-the-hunga-tonga-hunga-ha-apai-eruption-plume>





1 **The Cross Equatorial Transport of the Hunga Tonga-Hunga Ha'apai Eruption Plume**

2 M. R. Schoeberl & Yi Wang, Science and Technology Corporation, Columbia, MD, USA

3 R. Ueyama, NASA Ames Research Center, Moffett Field, CA, USA

4 G. Taha, Morgan State University, Baltimore, MD, USA

5 W. Yu, Hampton University, Hampton, VA, USA

6

7 Corresponding Author: Mark Schoeberl (mark.schoeberl@mac.com)

8

9 **Key Points**

- 10 • Following the eruption, cross-equatorial transport of the water vapor occurs even though
11 the meteorology does not appear to support this.
- 12
- 13 • IR cooling associated with the enhanced water vapor after the eruption likely generated
14 waves that produced the cross-equatorial flow.
- 15
- 16 • QBO-induced secondary circulation several months after the eruption also produced
17 cross-equatorial transport of water vapor.

18

19 **Plain Language Summary**

20 The Hunga Tonga-Hunga Ha’apai (HT) submarine volcanic eruption on January 15, 2022,
21 produced aerosol and water vapor plumes in the stratosphere. These plumes have persisted in the
22 Southern Hemisphere. Following the eruption, we believe that the strong water vapor cooling
23 forced an equatorial Rossby wave whose circulation pushed the eruption plume into the Northern
24 Hemisphere. Then, in April and May 2022, the descending quasi-biennial oscillation transported
25 more of the water vapor plume across the equator and widened the latitudinal extent of the
26 aerosol plume. The spring 2022 change in the HT plume distribution shows the importance of
27 forced Rossby waves and the QBO in stratospheric interhemispheric transport.

28

29 **Abstract**

30 On Jan. 15, 2022, the Hunga Tonga-Hunga Ha’apai (HT) eruption injected SO₂ and water into
31 the middle stratosphere. Shortly after the eruption, the water vapor anomaly moved northward
32 toward and across the equator. This northward movement appears to be due to a Rossby wave
33 forced by the excessive IR water vapor cooling. Following the early eruption stage, persistent
34 mid-stratospheric water vapor and aerosol layers were mostly confined to Southern Hemisphere
35 (SH) tropics (Eq. to 30°S). However, during the spring of 2022, the westerly phase of the
36 tropical quasi-biennial oscillation (QBO) descended through the tropics. The HT water vapor
37 and aerosol anomalies were observed to again split across the equator coincident with the descent
38 of the QBO shear zone. This split occurred because of the enhanced meridional transport
39 circulation associated with the QBO. Neither transport event can be reproduced using MERRA2
40 assimilated winds.

41

42 **Index Terms**

43 0340 Middle atmosphere dynamics

44 0341 Middle atmosphere: constituent transport and chemistry

45 0370 Volcanic effects

46

47 1. Introduction

48 The Hunga Tonga-Hunga Ha'apai (HT) (20.54°S, 178.3°W) erupted on Jan. 15, 2022, with a
49 volcanic explosivity index (VEI) of 5, comparable to Krakatoa eruption in 1883. As shown in
50 Microwave Limb Sounder (MLS) measurements (Millán et al., 2022, hereafter M22) and balloon
51 sondes (Vomel et al. 2022) a significant amount of water vapor was injected into the southern
52 hemisphere (SH) mid-stratosphere. HT also injected SO₂ which produced a distinctive aerosol
53 layer (Taha et al., 2022), although SO₂ injection was modest for an eruption of this size (Carn et
54 al., 2022; M22). The MLS estimated water injection was up to 146 Tg (M22) or ~10% of the
55 total stratospheric water vapor prior to the eruption. The water vapor and aerosol plumes from
56 the HT eruption have persisted in the southern tropical mid-stratosphere for months, and the
57 presence of water vapor led to a stratospheric cooling of ~ 4° K in March and April (Schoeberl et
58 al., 2022, hereafter S22) due to the increased outgoing IR radiation.

59
60 Trajectory simulations of the HT plume reported in S22 show that the plume should remain
61 almost entirely in the SH, yet observations of both the aerosols and water vapor in the mid-
62 stratosphere show the plume extending to 20°N. Below we show that there were two events
63 where water vapor was transported across the equator into the northern hemisphere (NH). The
64 first event occurred within a month of the eruption. This event also transported aerosols. The
65 second event was associated with descending QBO shear zone. Below we analyze both events,
66 starting with the QBO transport event.

67 2. Data sets

68
69
70 As discussed in S22, we use MLS v5 for ozone, N₂O, temperature and H₂O. The data quality for
71 the HT anomaly is detailed in M22 and MLS data is described in Livesey et al. (2021). The MLS
72 V5 algorithm quality flags and convergence alerts were set for some plume profiles in the week
73 or so after the eruption. However, even with the quality flag and convergence filters set, the data
74 look reasonable and generally agree with sonde and other validation data. We restrict our
75 constituent analysis to below 35 km. The MLS and OMPS data sets are averaged over 3 days and
76 then averaged onto a 5°x10° latitude-longitude grid. For aerosols, we use OMPS-LP level-2 V2.1
77 997 nm extinction-to-molecular ratio data (AE) from all three OMPS-LP slits (see Taha et al.,
78 2021). Taha et al. (2022) indicated that the standard V2.1 released data (used in this study)
79 provided the most accurate aerosol retrieval up to 36 km.

80
81 The Modern-Era Retrospective analysis for Research and Applications, Version 2 (MERRA2)
82 reanalysis winds, temperatures, and heating rates used in this study are described in Gelaro et al.,
83 (2017). The residual circulation is computed using the formulas in Andrews et al. (1987),
84 specifically Eq 3.5.5b for computing the residual vertical velocity (w^*) from the heating rate.
85 The upward residual circulation velocity magnitude from our computation agrees with analysis
86 of the water vapor tape recorder (Schoeberl et al., 2009). The continuity equation is then used to
87 compute the residual meridional velocity (v^*). MERRA2 data assimilation system does not
88 include the water vapor measurements from MLS and thus does not account for the additional
89 cooling from the water vapor anomaly (Coy et. al., 2022). To include that anomalous water
90 vapor cooling we compute the total IR heating rate using 2022 MLS observed trace gases and
91 temperatures using the radiative transfer model (RTM) described by Mlawer et al. (1997). We

92 then we rerun the heating rate calculation assuming pre-eruption concentration of water vapor (~
93 4 ppm). We compute the difference in radiative heating between the two computations and add
94 that difference to the MERRA2 net heating rate, then recompute w^* . At 15°S, 26.8 km the
95 MERRA2 residual circulation is upward with ~ 0.1 cm/s in January, decreasing to 0.03 cm/s in
96 October. With the addition of the water vapor cooling the residual circulation is slower by 5% in
97 January. The circulation is further reduced by ~20% by mid-February through March then the
98 water vapor cooling effect fades through July. Over the equator the reduction in w^* is only a
99 few percent over this period.

101 3. Analysis

102
103 In the next two sections we address the two cross equatorial constituent mixing events.

104 3.1 Cross Equatorial Transport associated with the QBO

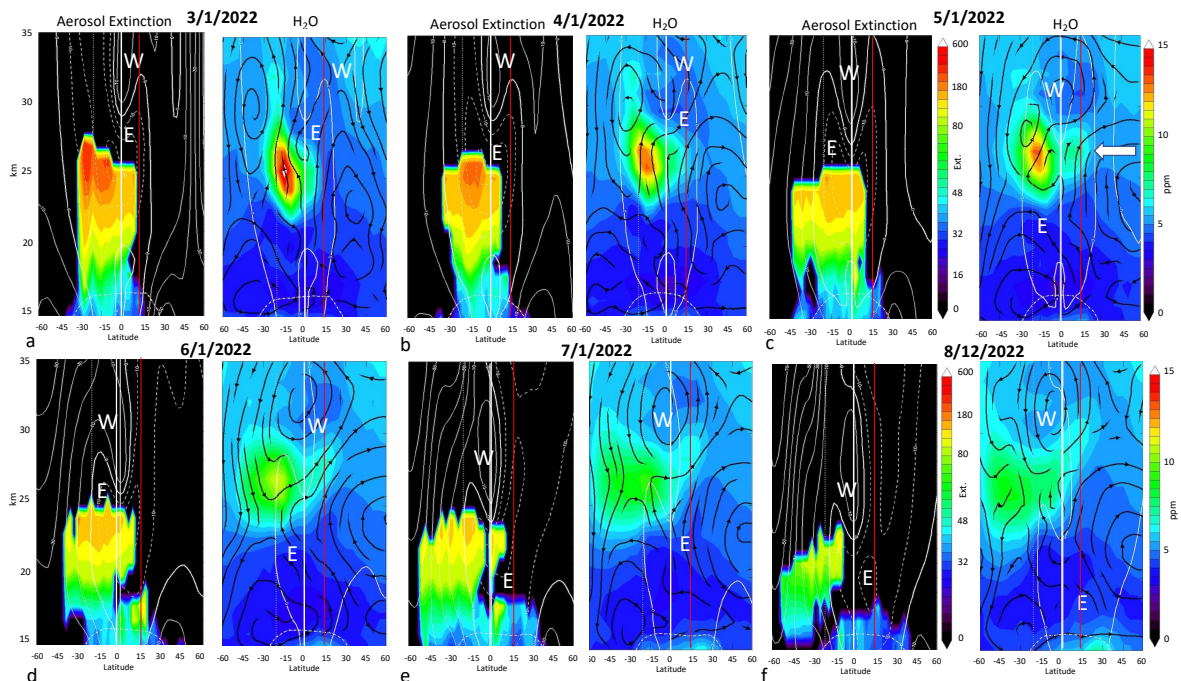
105
106
107 Unrelated to the HT eruption, during the 2022 spring and summer, the tropical stratospheric
108 winds switched from easterly to westerly due to the quasi-biennial oscillation (QBO) (see review
109 by Baldwin et al., 2001). The descending westerly phase QBO produces a secondary circulation
110 with downwelling at the equator – roughly the locus of the zero-wind line - and upwelling north
111 and south of the equator (Plumb and Bell, 1982). This secondary circulation will alter the
112 distribution of trace gases such as ozone and water vapor. The induced circulation contributes to
113 the mixing of the lower stratospheric trace gases within the tropics, and between the hemispheres
114 as is evident in observational data sets (Anstey et al., 2022; Baldwin et al., 2001; Randel et al.,
115 1998). The simple models of the QBO assume that the secondary circulation is symmetric about
116 the equator so cross equatorial transport would not be possible in that framework, but the
117 observed structure of the QBO circulation is not equatorially symmetric and the cross-equatorial
118 circulation can be quite strong (Randel et al., 1999). The QBO circulation asymmetry is likely
119 due to hemispheric differences in the upward gravity wave momentum flux that contributes to
120 the QBO (Anstey et al., 2022; Baldwin et al., 2001).

121
122 Figure 1a-f shows the evolution of the OMPS-LP aerosol extinction (Taha et al, 2021) and MLS
123 zonal mean water vapor. The MERRA2 zonal mean wind is also shown along with the residual
124 circulation streamlines. The observations are shown at the first of each month except for August
125 where we show the 12th, because OMPS-LP was offline at beginning of the month. We begin in
126 March when the HT water vapor field becomes zonally well mixed as indicated by the MLS
127 observations (Fig. 2a). The initial water vapor and aerosol distribution is primarily south of
128 10°N. The figure shows that the water vapor is concentrated mostly above 20 km where the
129 warmer stratosphere can support higher concentrations (S22). The aerosols are initially
130 distributed from the tropopause to approximately the same altitude as the water vapor, but the
131 two distributions slowly separate in time with the water vapor anomaly rising while the peak
132 altitude of the aerosol anomaly descends as noted in S22.

133
134 The Fig. 1 sequence shows the descent of the tropical QBO westerlies as see in the downward
135 propagation of the zero-wind line. Between March 1 and April 1 there is little descent of the
136 equatorial westerlies above about 30 km. Then, beginning in April, the westerlies begin to
137 descend rapidly. By May 1, the top of the aerosol distribution has spread deeper into the SH and

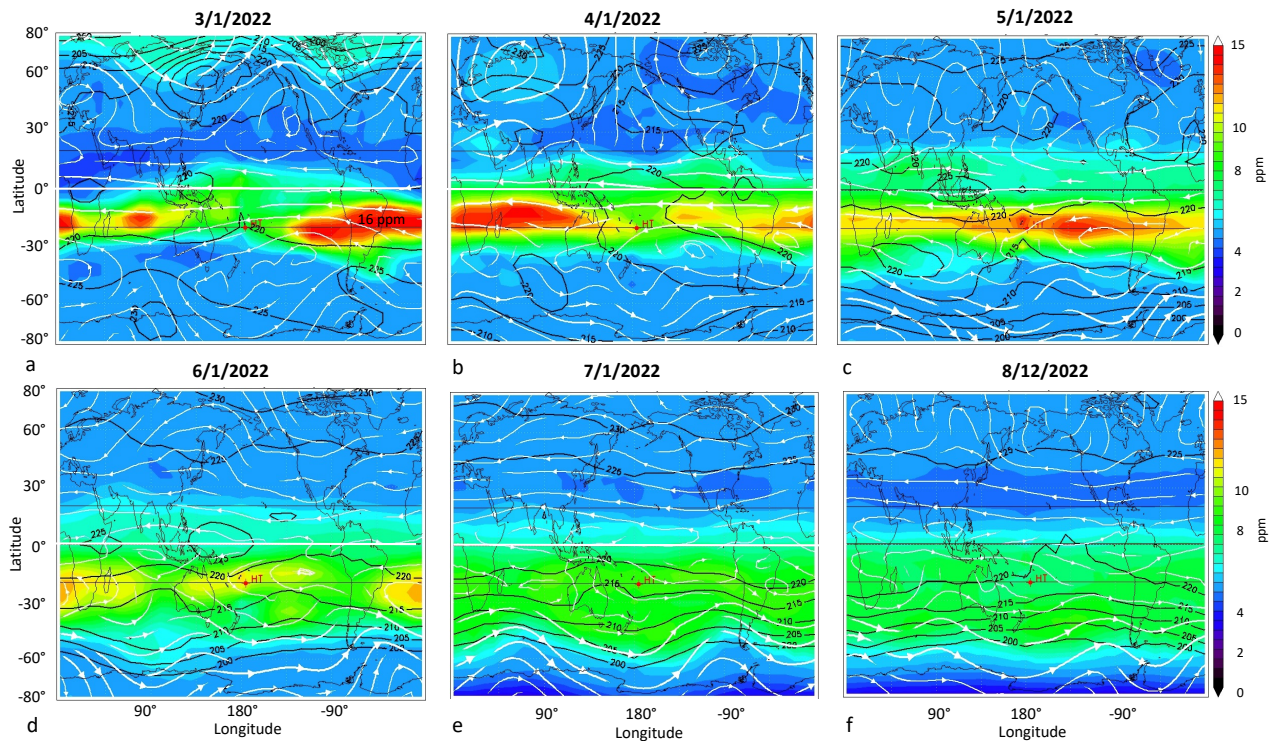
138 a secondary maximum in water vapor has appeared in the NH (see arrow). The residual
 139 streamlines shown overlaid on the water vapor plots provide an explanation for the changing
 140 aerosol and water vapor distributions. In March, the $\sim 20^{\circ}\text{S}$ upward transport of water vapor is
 141 consistent with the residual circulation (S22). In April, the streamlines shift, and the residual
 142 circulation begins to transport water vapor toward the north. By May 1 (Fig. 1c), a lobe of water
 143 vapor has formed in the Northern Hemisphere (NH) moving north of 15°N . The northward
 144 residual circulation is still present on May 1 but has weakened, although the water vapor
 145 anomaly continues to slowly expand northward. At lower altitudes the southern branch of the
 146 residual circulation is transporting the aerosol distribution further south.

147
 148 By July, above the tropical zero-wind line within the westerly wind regime, the ascending branch
 149 of the residual circulation in the NH tropics reinforces a descending branch in the SH tropics.
 150 This circulation cell transports dry air downward into the HT anomaly while pulling the northern
 151 edge of the anomaly upward. This transport creates the U-shaped structure in water vapor seen in
 152 July and August. The aerosol anomaly, which has continued to settle throughout this sequence,
 153 does not show the cross-equatorial transport seen in the water vapor field. The residual
 154 circulation at the lower altitude does not have a northward (poleward) component during this
 155 period, so the aerosols do not spread north of 15°N .



156
 157 *Figure 1 Sequence of zonal mean 997 nm aerosol extinction and water vapor plots starting*
 158 *March 1 (a), April 1, (b), etc. Because OMPS-LP was not operational on August 1, we plot*
 159 *August 12 in part f. The plots are the individual days; the data is averaged over 3 adjacent days.*
 160 *The zonal wind is shown overlaid on the aerosol plots as white contours. The ‘W’ and ‘E’*
 161 *indicate westerly and easterly regimes. The residual circulation streamlines (black) are overlaid*
 162 *on the water vapor figures along with the zero-wind line (white contour). The arrow in Fig. 1c*
 163 *shows the enhanced spreading of the water vapor below the QBO zero-wind line. Vertical white*
 164 *and red lines indicate 0° and 15°N for reference.*

165 The upward propagating tropical waves that produce QBO deposit their momentum in the shear
 166 zone centered on the zero-wind line. As wave momentum is deposited in the shear zone, the
 167 zonal wind speed changes, moving the shear zone downward. Observations and models show
 168 that the secondary circulation surrounding the QBO momentum deposition region extends ~ 5
 169 km below the shear zone (Baldwin et al., 2001) and QBO wind anomalies extend horizontally to
 170 $\sim 15^\circ$ on either side of the equator (Dunkerton and Delisi, 1985). We can interpret the changes in
 171 water vapor in terms of the QBO induced transport circulation as follows: Between March 1 and
 172 April 1, the QBO descent is very slow, which means that there is little wave momentum being
 173 deposited at upper levels. The QBO secondary circulation is weak, and the stratospheric
 174 circulation is dominated by the seasonal Brewer-Dobson circulation. The HT water vapor
 175 anomaly is confined mostly to the SH at this stage. Starting in April, the westerlies begin to
 176 descend, the meridional residual circulation below the zero-wind line begins to transport water
 177 vapor northward across the equator. Note that the residual circulation in the tropics, which is a
 178 combination of seasonal and QBO circulations, is not symmetric across the equator and the
 179 northward transport cell extends into the SH (Randel et al., 1999. In 2022, this asymmetry may
 180 have been amplified by additional water vapor cooling in the SH (S22). As the zero-wind line
 181 continues to descend into the HT plume, the residual circulation weakens, and transport slows
 182 (June, July). This weakening can be partly attributed to a seasonal change in the Brewer-Dobson
 183 circulation which is strongest during boreal winter (Plumb, 2002). Thus, the observed changes in
 184 the HT water vapor distribution are broadly consistent with the circulation surrounding the
 185 descending QBO (Plumb and Bell, 1982, Baldwin et al., 2001) combined with the seasonally
 186 changing Brewer-Dobson circulation (Randel et al., 1999, Gray and Dunkerton, 1990).
 187



188
 189 *Figure 2 Maps of the MLS water vapor at 26.8 km (~ 21.5 hPa) using 3 days of data centered on*
 190 *the date shown. Temperatures (also from MLS) are shown with black contours. The streamlines*
 191 *(white arrows) are generated using MERRA2 winds. The dates correspond to those in Fig. 1.*

192 From the simple models of the QBO, we expect that waves to amplify as the shear zone
193 approaches from above, and then wave amplitudes should decrease as the shear zone passes. The
194 change in wave activity occurs due to conservation of wave action density – the wave energy
195 divided by the frequency (Andrews et al., 1987, Eq 4A.12). As the wave propagates upward
196 toward its critical line, the group velocity decreases, and the wave amplitude increases. This
197 should enhance the variance in trace gas fields if a tracer gradient is present. Figure 2 shows
198 maps of the MLS water vapor distribution and temperatures at 26.8 km (~21.5 hPa) along with
199 streamlines from MERRA2 winds. The H₂O distribution on April 1 shows a wave structure at the
200 northern edge of the anomaly, and the temperature and streamlines show more non-zonal
201 structure. By May 1 the water vapor distribution uniformly extends to 20°N and the wave
202 structures in tropical wind and temperature fields have decreased. The wave structure seen on
203 April 1 might be expected from the amplification of the Kelvin wave as it approaches the critical
204 line. Then, in the subsequent months (June–August), the water vapor distribution becomes more
205 zonally uniform along with the wind and temperature fields. We have examined the time
206 variation of the water vapor variance at 26.8 km and indeed it increase as the QBO moves
207 downward to this altitude and then abruptly decreases with the passage of the shear zone. The
208 equatorial seasonal upward residual circulation also switches from ascending to descending as
209 the QBO shear zone passes then returns to ascending as expected from the simple QBO models
210 (Plumb and Bell, 1982).

211

212 *3.2 Cross Equatorial Transport Shortly after the Eruption*

213

214 Figure 3 shows maps of water vapor and streamlines at 26.8 km for selected days following the
215 eruption. Rather than average the data over three days, we show the location of MLS profiles
216 and the water vapor mixing ratio. The maximum water vapor is shown at the lower left of each
217 figure. Figure 3a shows the distribution on Jan 16. As noted by Millán et al. (2022), MLS scans
218 do not completely catch the locally concentrated plume. Figure 3b (Jan. 20) shows the anomaly
219 moving toward the equator roughly following the streamlines. By Jan 23 the anomaly has
220 crossed the equator and reached 10°N even though streamlines are mostly zonal. The MERRA2
221 meridional flow at this altitude is < 2 m/s at ±15°N which means that it would take ~10 days for
222 the plume to transit from 5°S to 10°N, but this transit took place in about 3-4 days. On Jan. 26
223 the anomaly has reached 10°N. Because of the strong meridional wind shear, and faster winds at
224 the equator, move the equatorial portion ahead of the slower moving higher latitude component
225 (Figs. 3d-3f).

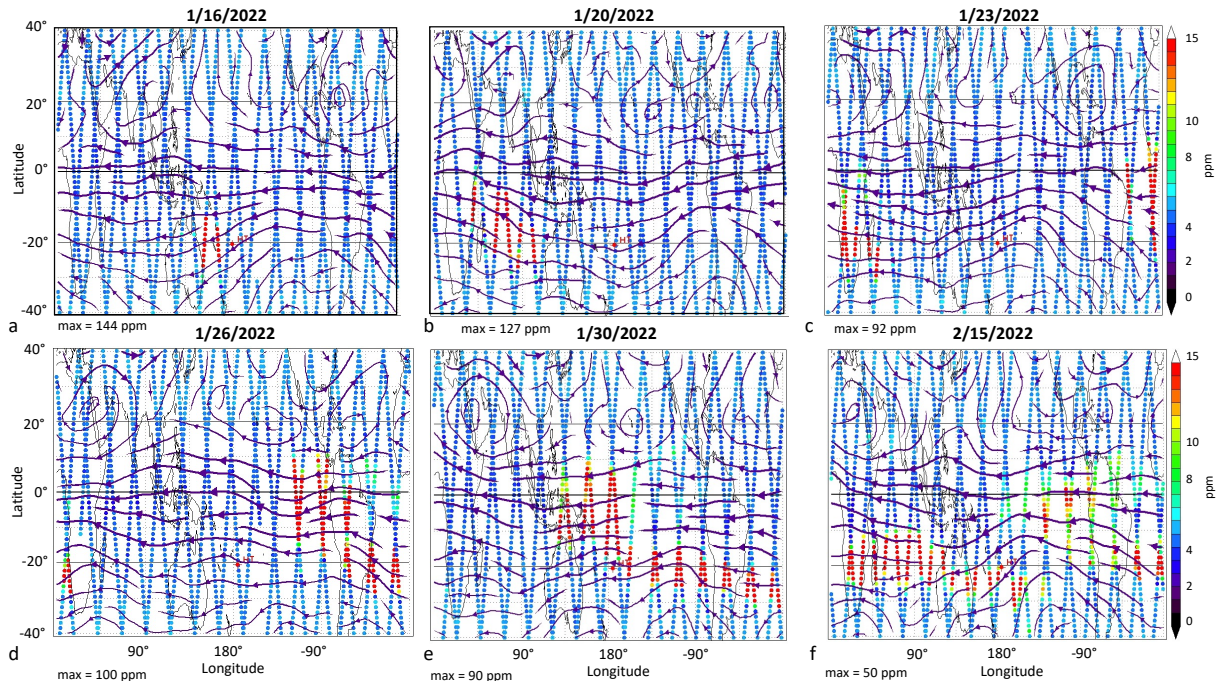
226

227 Why did the HT water vapor anomaly move more rapidly to the north between Jan. 20 and Jan.
228 23? One possible explanation for the movement of the plume toward the equator is that the IR
229 cooling from the water vapor anomaly excited a Rossby wave that advected the water vapor
230 anomaly toward the equator. The simple circulation models of thermally forced equatorial
231 Rossby waves provided by Gill (1980, Fig. 3) would apply. In this scenario, the IR cooling by
232 the water vapor anomaly creates a local pressure anomaly which excites a Rossby wave, creates
233 cross equatorial flow, which advects part of the anomaly across the equator. Because this cooling
234 is not included in the MERRA2 reanalysis (because the MLS water vapor is not assimilated), the
235 strength of the MERRA2 meridional wind is probably underestimated. We have computed the
236 additional IR cooling for Jan 19, using the RTM, and at 27.5 km it is ~3K/day reaching ~5K/day
237 at 30 km. Our estimate of the radiative forcing is in agreement with Silletto et al. (2022) who

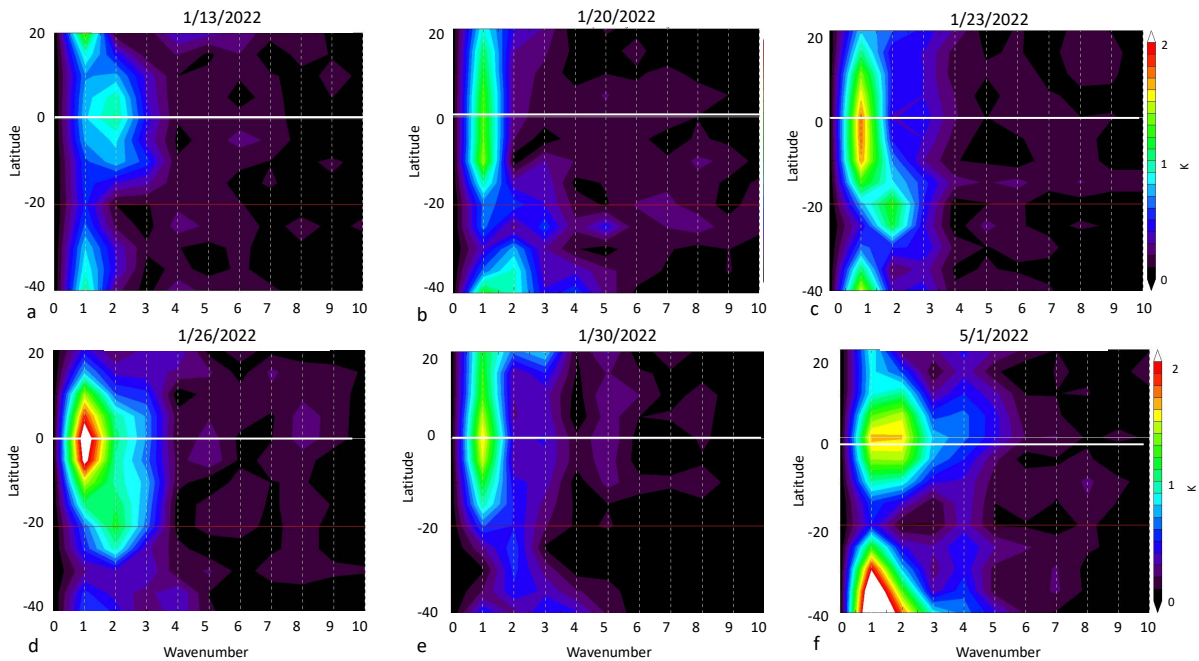
238 also noted that the aerosol plume has almost no net radiative impact. This magnitude of localized
239 cooling just off the equator is sufficient to force the Rossby wave (Gill, 1980). After the plume
240 is advected toward the equator and the water vapor distribution becomes more zonal, the non-
241 zonal cooling rate would decrease and the Rossby wave amplitude would decrease as well.
242

243 A zonal spectral analysis of the temperature fields provides more insight. Figure 4 shows a zonal
244 wavenumber spectrum at 26.8 km using 3-day average MLS perturbation temperatures. Fig. 4a
245 shows the pre-eruption wave amplitudes vs. latitude on Jan. 13, indicating that the ambient
246 waves are weak, with a ~1K amplitude Kelvin wave centered on the equator. On Jan. 20 (Figs.
247 4b, 3b), just following the eruption, conditions are immediately different. The thermal amplitude
248 of wave one has nearly doubled north of the HT eruption latitude. The thermal disturbance
249 associated with the spatially narrow plume spreads energy into the higher wavenumbers at 20°S.
250 By Jan. 26, (Fig. 4c, 3c) wave one has increased to 1.5K at about 5°S, and a wave two
251 disturbance has also formed at the HT latitude. By Jan. 26 (Fig. 4d, 3d), the wave one amplitude
252 has increased to > 2K and wave 2 has reached 1.5 K. The waves subsequently begin to decrease
253 in amplitude as seen on Jan. 30 (Fig. 4e, 3e). Wave amplitudes continue to decrease during
254 February (not shown).
255

256 The thermal wavenumber analysis is consistent with the idea that H₂O IR cooling generates
257 equatorial Rossby waves shortly after the eruption. We can make a rough estimate of the
258 enhanced meridional circulation (v') generated by the wave using the thermal wind equation and
259 assuming that the heating anomaly has the vertical scale of a scale height (~ 7km). v' is given by
260 $v' = mRT'/f$, where f is the Coriolis frequency at 15°S, R is the dry air gas constant, m is the zonal
261 wavenumber and T' is the temperature. Using $T' = 2$ K, $v' \sim 2.5$ m/s. Adding this to the
262 background meridional flow of 2 m/s, the transit time to move the water vapor from 5°S to 15°N
263 is 4.5 days. This is much closer to the observed anomaly transit time from Jan 20-23 period.
264 Finally, to connect with the QBO discussion in section 3.1, Fig. 4f shows the wave amplitudes on
265 April 1. The figure clearly shows wave amplification as the QBO shear line approaches 26 km
266 when compared to Figure 4a.
267



268
 269 *Figure 3 Maps of MLS observed water vapor anomaly at 26.8 km following the HT eruption. The*
 270 *peak water vapor mixing ratio is indicated at the lower left of each figure. Streamlines from*
 271 *MERRA2 are shown as arrows.*



272
 273 *Figure 4 MLS temperature wave amplitudes at 26.8 km vs latitude. Zonal mean temperature is*
 274 *removed. Dates are indicated above each plot. Red line indicates the latitude of HT, white line is*
 275 *the equator. Parts b-e correspond to figure 4b-e. Wave 0, the zonal mean, is removed.*

276

277 4. Summary and Discussion

278 The HT injection of aerosols and water into the mid-stratosphere provides an unprecedented
279 opportunity to examine our understanding of tropical stratospheric dynamics and
280 interhemispheric transport of trace gases. Trajectory simulations of the plume spread show
281 almost no mid-stratospheric transport across the equator during first 5 months after the eruption
282 (S22); nonetheless, at least two cross equatorial transport events occurred. The first, shortly after
283 the eruption and the second during April and May 2022. Explanation for these events is given in
284 this paper.

285
286 The initial HT plume moved $\sim 30^\circ$ northward within the first few weeks after the eruption (Fig.
287 3) even though the pre-eruption flow was approximately zonal with weak wave activity at
288 tropical latitudes. The northward advection of the plume may have resulted from strong H₂O IR
289 cooling of the plume, and the subsequent non-zonal radiative cooling would force an equatorial
290 Rossby wave response (Gill, 1980). The resulting cross equatorial flow would have transported
291 the plume meridionally. Wavenumber analyses of MLS temperatures show a coincidental rapid
292 increase in wave one and two across throughout tropics, consistent with this hypothesis. The
293 meridional cross-equatorial velocity may have more than doubled due to the presence of the
294 wave. By the end of January, the forced Rossby wave subsides as the water vapor plume shears
295 out and the localized (non-zonal) forcing decreases.

296
297 During March, the QBO shear zone began to descend through the tropics switching the zonal
298 winds from easterlies to westerlies in the mid-stratosphere. The induced circulation produced
299 by wave momentum deposition combined with the Brewer-Dobson circulation produces a
300 second cross-equatorial transport event. This event is most evident at ~ 26 km where the
301 meridional water vapor gradient is large. The QBO transport both observed in the MLS water
302 vapor mixing ratios, and as diagnosed through the residual circulation, is consistent with earlier
303 analyses of QBO dynamics (Baldwin et al., 2001; Randel et al., 1999). However, the circulation
304 well below the QBO shear zone appears to prevent a similar spread in the aerosol distribution.

305
306 The fact that these two transport events were not reproduced by trajectory simulations (S22)
307 suggests the need for additional improvements in MERRA2 tropical dynamics, and the need for
308 stratospheric water vapor assimilation – at least during the HT period. Finally, although the SH
309 and NH tropical stratospheres appear to be relatively isolated under normal conditions (Stolarski
310 et al., 2014), the evolution of the HT plume reveals that the QBO can play an important, albeit
311 episodic, role in trace gas exchange between the two hemispheres.

312 **Acknowledgements**

313 This work was supported under NASA grants NNX14AF15G, 80NSSC21K1965 and
314 80NSSC20K1235

315 .

316

317 **Open Research**

318 MERRA-2 Reanalysis data. Gelaro et al. (2017). MERRA-2 data are obtained from the Global
319 Modeling and Assimilation Office (GMAO), *inst3_3d_asm_Cp: MERRA-2 3D IAU State,*
320 *Meteorology Instantaneous 3-hourly (p-coord, 0.625x0.5L42), version 5.12.4* at <https://doi.org/>

322 10.5067/WWQSXQ8IVFW8. The data are public with unrestricted access (registration
323 required).
324
325 The RTM used to estimate H₂O cooling rates is from Atmospheric and Environmental Research
326 and can be freely downloaded at http://rtweb.aer.com/rrtm_frame.html.

327
328 OMPS-LP data, Taha et al. (2021), is available at
329 https://disc.gsfc.nasa.gov/datasets/OMPS_NPP_LP_L2_AER_DAILY_2/summary ,
330 DOI: <https://doi.org/10.5067/CX2B9NW6FI27> The algorithm is documented in Taha et al.
331 (2021). Data are public with unrestricted access (registration required).
332
333 Aura MLS Level 2 data, Livesey et al. (2021) JPL D-33509 Rev. C, is available at
334 <https://disc.gsfc.nasa.gov/datasets?page=1&keywords=AURA%20MLS>
335 The temperature data is available at
336 https://acdisc.gesdisc.eosdis.nasa.gov/data/Aura_MLS_Level2/ML2T.004/
337 The V4 water vapor data is available at
338 https://acdisc.gesdisc.eosdis.nasa.gov/data/Aura_MLS_Level2/ML2H2O.004/
339 The V5 water vapor data is available at
340 https://acdisc.gesdisc.eosdis.nasa.gov/data/Aura_MLS_Level2/ML2H2O.005/
341
342
343

344

345 **References**

346 Anstey, J.A., *et al.* (2022). Impacts, processes, and projections of the quasi-biennial
347 oscillation. *Nat. Rev. Earth Environ.*, 3, 588–603, <https://doi.org/10.1038/s43017-022-00323-7>

348

349 Baldwin *et al.*, (2001). The quasi-biennial oscillation, *Revs. of Geophys*, 39, 179-229,
350 <https://doi.org/10.1029/19999RG000073>.

351

352 Carn, S. A., N. A. Krotkov, B. L. Fisher, and C. Li, (2022). Out of the blue: volcanic SO₂
353 emissions during the 2021-2022 Hunga Tonga – Hunga Ha’apai eruptions,

354 <https://www.essoar.org/pdfjs/10.1002/essoar.10511668.1>

355

356 Coy, L., P. Newman, K. Wargan, G. Partyka, S. Strahan, and S. Pawson, (2022). Stratospheric
357 Circulation Changes Associated with the Hunga Tonga-Hunga Ha'apai Eruption, *Geophys. Res.*

358 *Let.*, 49, <https://www.essoar.org/doi/abs/10.1002/essoar.10512388.1>

359

360 Dunkerton, T. J., and D. P. Delisi (1985). Climatology of the equatorial lower stratosphere, *J.*
361 *Atmos. Sci.*, 42, 376-396.

362

363 Gelaro, R., *et al.* (2017). The Modern-Era Retrospective Analysis for Research and Applications,
364 Version 2 [Dataset], *J. Climate*, 30, 5419-5454, <https://doi.org/10.1175/jcli-d-16-0758.1>.

365

366 Gill, A. E., (1980). Some simple solutions for heat-induced tropical circulation, *Quart. J. R. Met.*
367 *Soc.*, 106, 447-462.

368

369 Gray, L. J., and T. J. Dunkerton, (1990). The role of the seasonal cycle in the quasi-biennial
370 oscillation of ozone, *J. Atmos.Sci.*,47, 2429-2451.

371

372 Livesey, N., Read, W.G., Wagner, P.A., Froidevaux, L., Santee, M.L., Schwartz, M.J. *et al.*
373 (2021) Earth Observing System (EOS) Aura Microwave Limb Sounder (MLS) version 5.0x level
374 2 and 3 data quality and description document, JPL D-105336 Rev

375 A. https://mls.jpl.nasa.gov/data/v5-0_data_quality_document.pdf

376

377 Millán, L. *et al.*, (2022). The Hunga Tonga-Hunga Ha’apai Hydration of the Stratosphere,
378 *Geophysical Research Letters*. 49, e2002GL099381, <https://doi.org/10.1029/2022GL099381>

379

380 Mlawer, E.J., S.J. Taubman, P.D. Brown, M.J. Iacono and S.A. Clough (1997). RRTM, a
381 validated correlated-k model for the longwave. *J. Geophys. Res.*, **102**, 16,663-16,682.

382

383 Plumb R. A. and R. C. Bell (1982). A model of the quasi-biennial oscillation on an equatorial
384 beta-plane, *Quart. J. R. Met. Soc.*, 108, 335-352.

385

386 Plumb, R. A. (2002). Stratospheric transport, *J. Meteor. Soc. Japan*, 80, 793-809.

387

388 Proud, S. R., Prata, A., & Schmauss, S. (2022). The January 2022 eruption of Hunga Tonga-
389 Hunga Ha’apai volcano reached the mesosphere. *Science*, 378, 554-557.
390
391
392 Randel, W. J., F. Wu, J. M. Russel III, A. Roche, and J. Waters, (1998) Seasonal cycles and
393 QBO variations in stratospheric CH₄ and H₂O observed in UARS HALOE data, *J. Atmos. Sci.*,
394 55, 163-185, [https://doi.org/10.1175/1520-0469\(1999\)056<0457:GQCDFU>2.0.CO;2](https://doi.org/10.1175/1520-0469(1999)056<0457:GQCDFU>2.0.CO;2)
395
396
397 Randel, W. J., F. Wu, R. Swinbank, J. Nash, and A. O'Neill (1999). Global QBO circulation
398 derived from UKMO stratospheric analyses *J. Atmos. Sci.*, 56, 457-474.
399 [https://doi.org/10.1175/1520-0469\(1998\)055<0163:SCAQVI>2.0.CO;2](https://doi.org/10.1175/1520-0469(1998)055<0163:SCAQVI>2.0.CO;2)
400
401 Schoeberl, M. R., A. R. Douglass, R. S. Stolarski, S. Pawson, S. E. Strahan, and W. Read (2008).
402 Comparison of lower stratospheric tropical mean vertical velocities, *J. Geophys. Res.*, 113,
403 D24109, <https://doi.org/10.1029/2008JD010221>
404
405 Schoeberl, M. R., Wang, Y., Ueyama, R., Taha, G., Jensen, E., & Yu, W. (2022).
406 Analysis and impact of the Hunga Tonga-Hunga Ha'apai stratospheric water vapor plume.
407 *Geophysical Research Letters*, 49, e2022GL100248. <https://doi.org/10.1029/2022GL100248>
408
409 Silletto, P., A. Podglagen, R. Belhadji, M. Boichu, E. Carboni, J. Cuesta, C. Duchanp, C. Kloss,
410 R. Siddans, N. Begue, L. Blarel, F. Jegou, S. Khaykin, H-B. Renard, and B. Legras, (2022), The
411 unexpected radiative impact of the Hunga Tonga eruption of January 15, 2022, *Commun Earth*
412 *Environ* **3**, 288 (2022). <https://doi.org/10.1038/s43247-022-00618-z>
413
414 Stolarski, R. S., D. W. Waugh, L. Wang, L. D. Oman, A. R. Douglass, and P. A. Newman
415 (2014). Seasonal variation of ozone in the tropical lower stratosphere: Southern tropics are
416 different from northern tropics, *J. Geophys. Res. Atmos.*, 119, 6196–6206,
417 <https://doi.org/10.1002/2013JD021294> .
418
419 Taha, G., R. Loughman, T. Zhu, L. Thomason, J. Kar, L. Rieger, and A. Bourassa (2021). OMPS
420 LP Version 2.0 multi-wavelength aerosol extinction coefficient retrieval algorithm, *Atmos.*
421 *Meas. Tech.*, 14, 1015–1036, <https://doi.org/10.5194/amt-14-1015-2021>
422
423 Taha, G., R. Loughman, P. Colarco, T. Zhu, L. Thomason, G. Jaross (2022). Tracking the 2022
424 Hunga Tonga-Hunga Ha'apai aerosol cloud in the upper and middle stratosphere using space-
425 based observations, *Geophys. Res. Lett.*, <https://doi.org/10.1029/2022GL100091>
426
427 Vömel, H., S. Evan, and M. Tully (2022). Water vapor injection into the stratosphere by Hunga
428 Tonga-Hunga Ha’apai, *Science*, 377,1444-1447.
429
430

Figure 1.

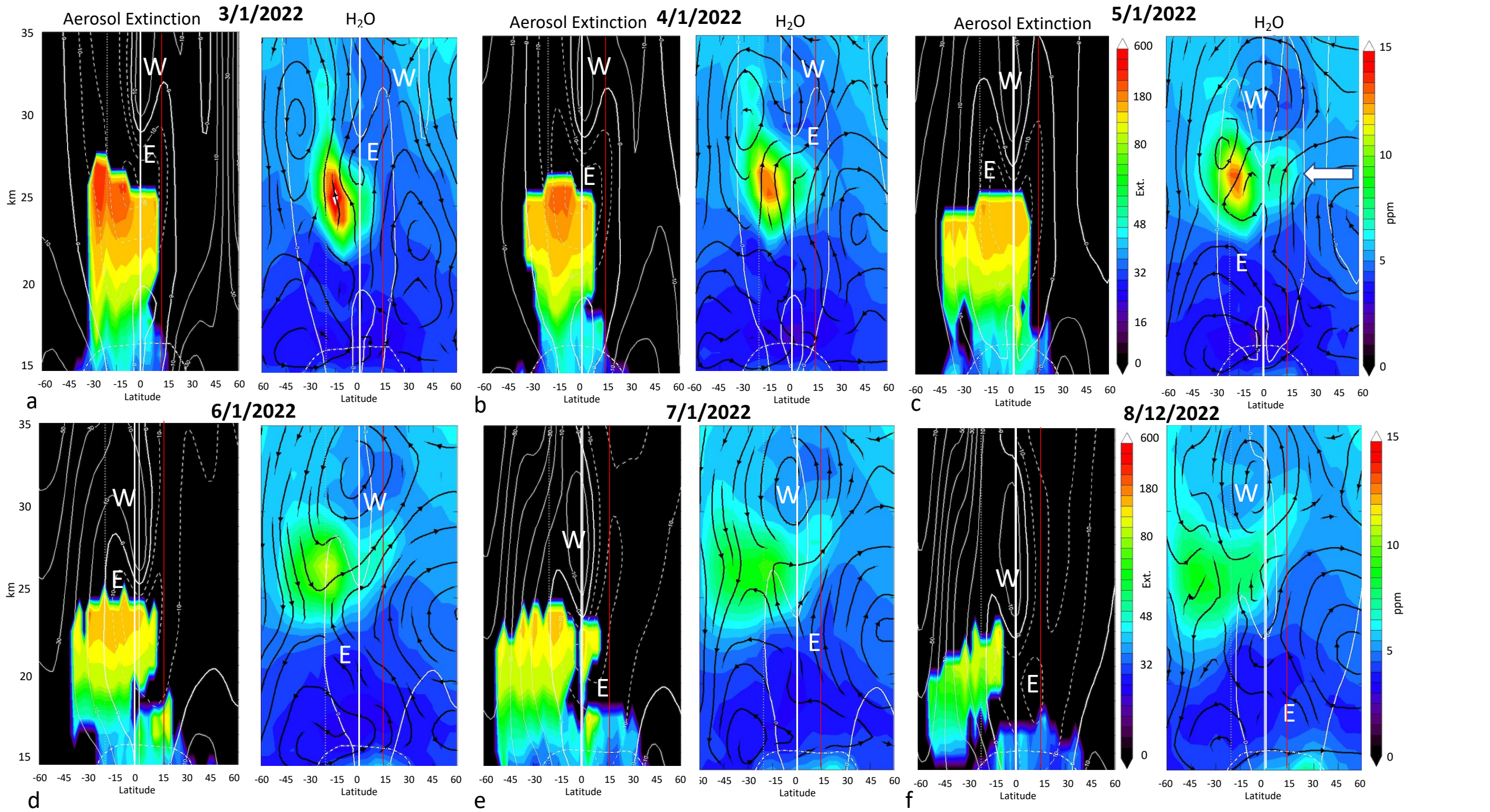
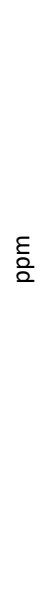
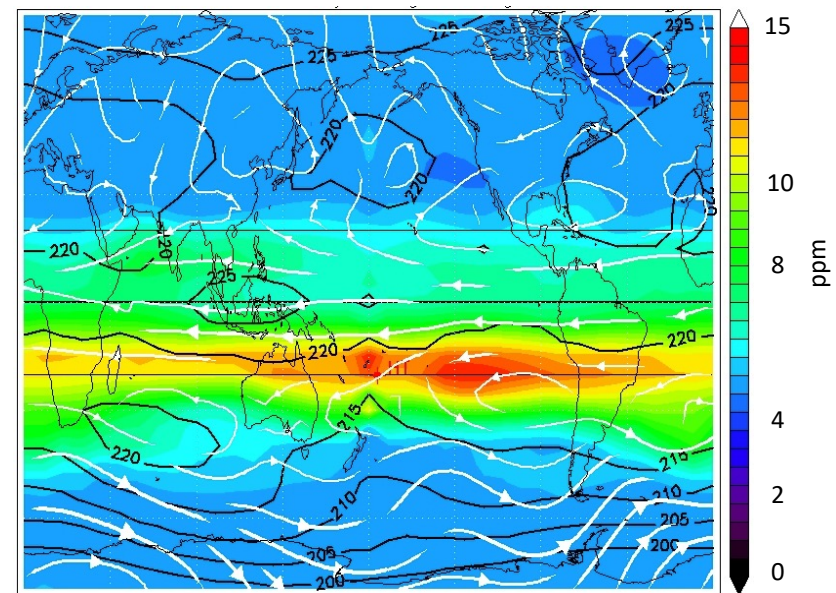
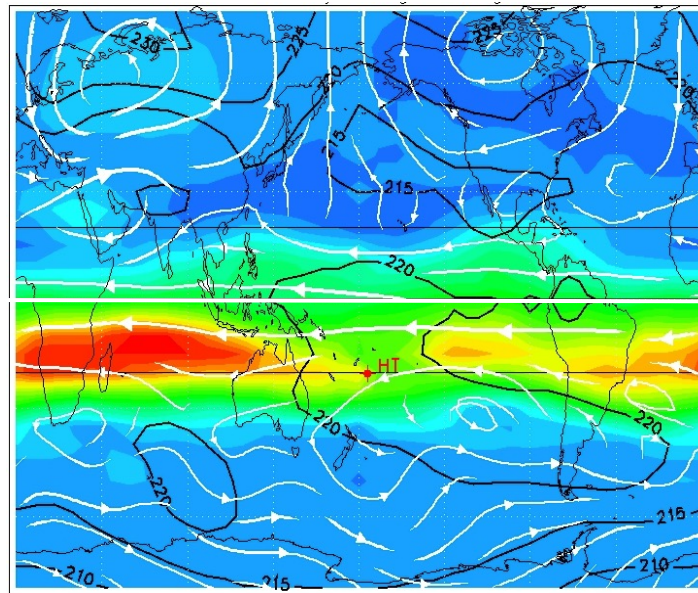
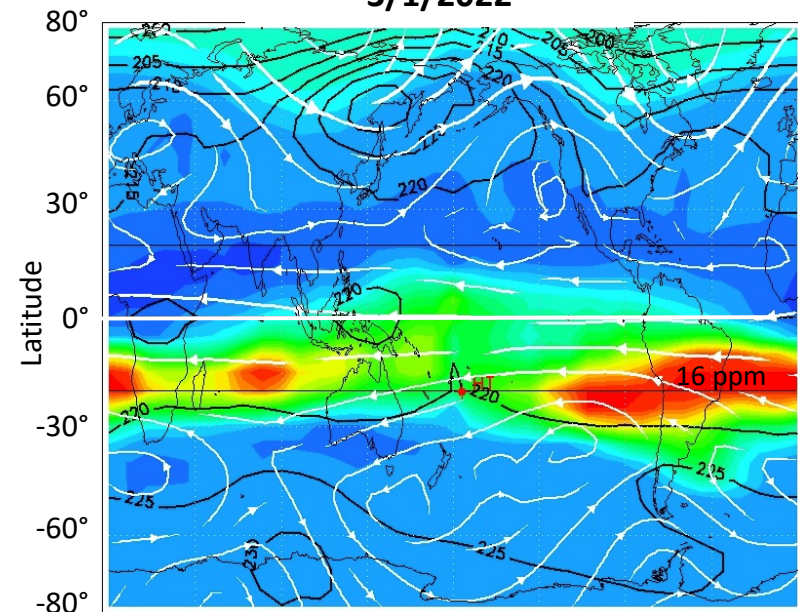


Figure 2.

3/1/2022

4/1/2022

5/1/2022



a

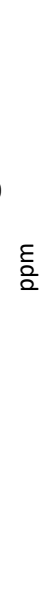
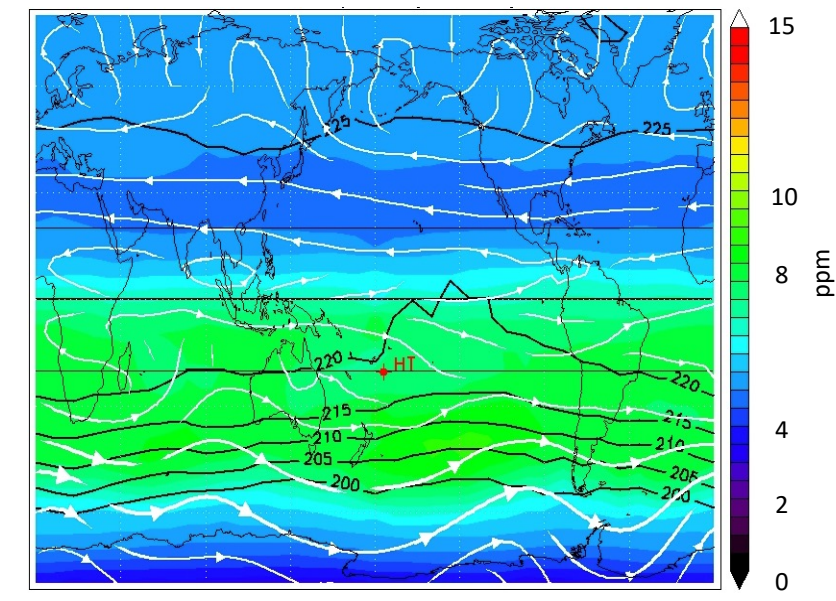
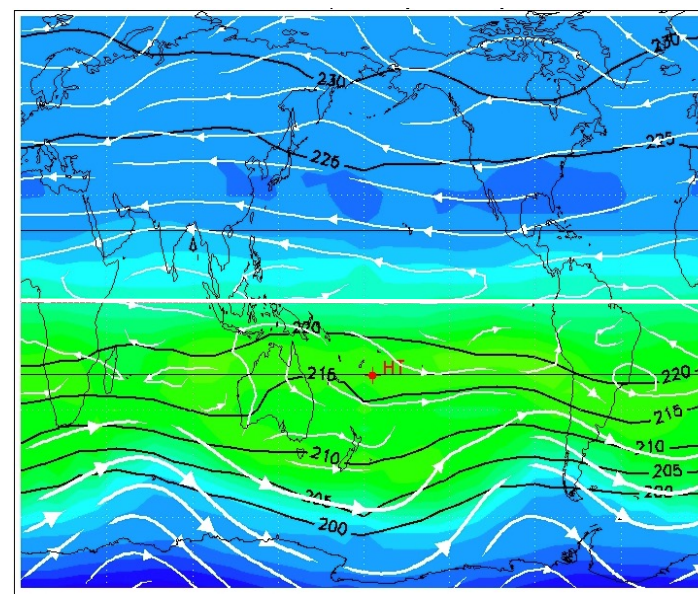
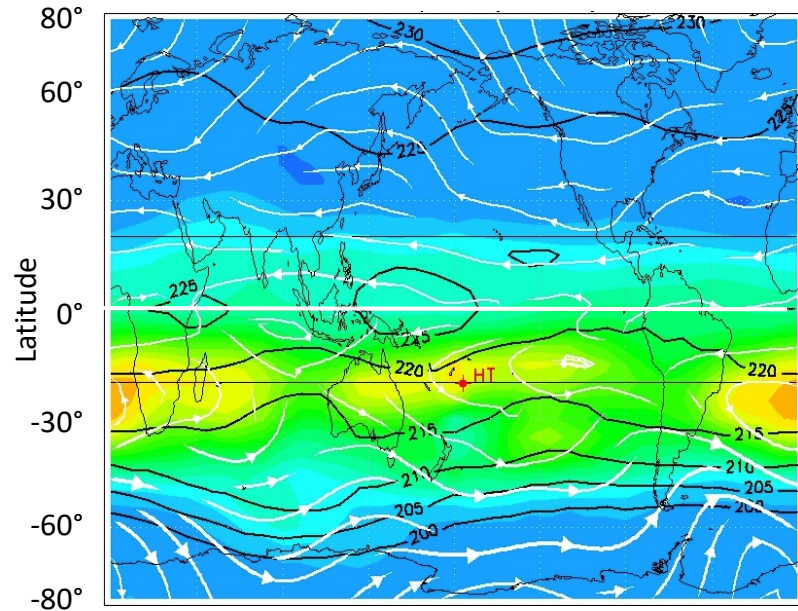
b

c

6/1/2022

7/1/2022

8/12/2022



d

e

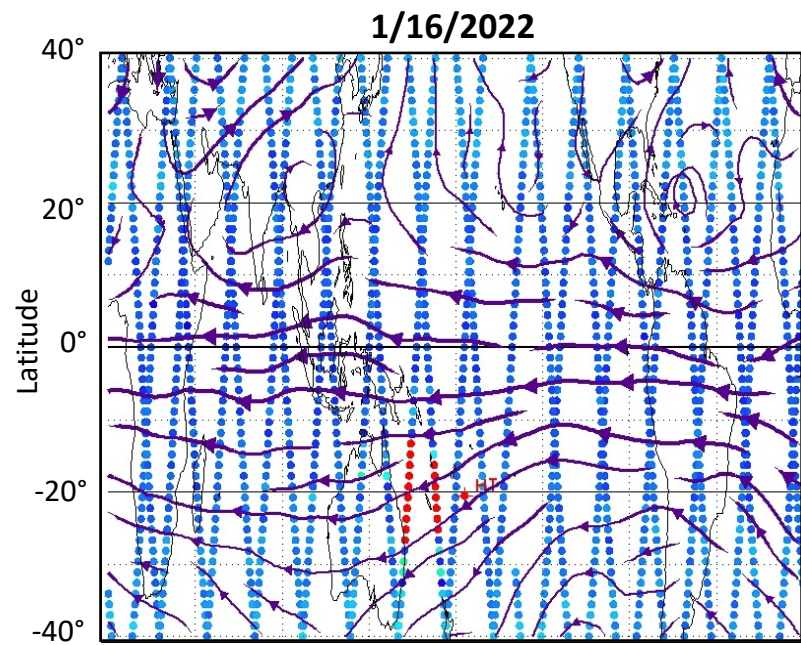
f

90° 180° -90°
Longitude

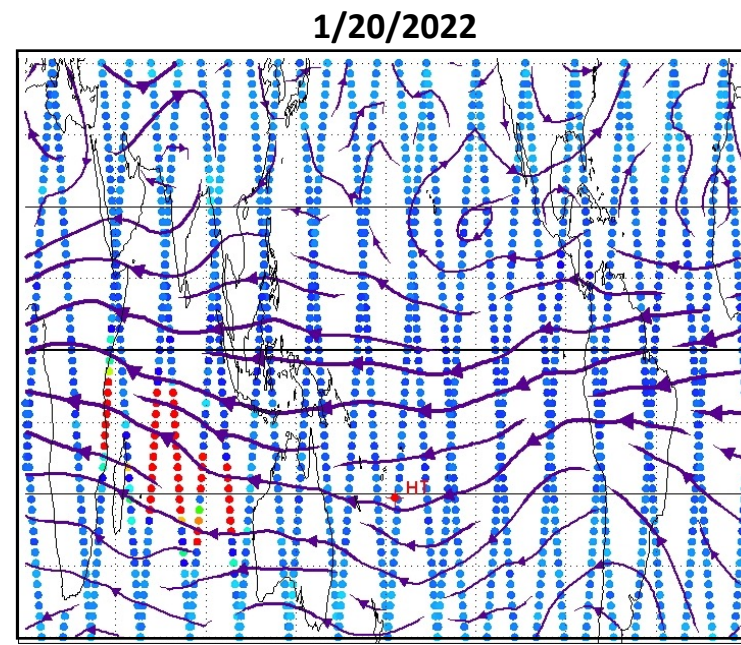
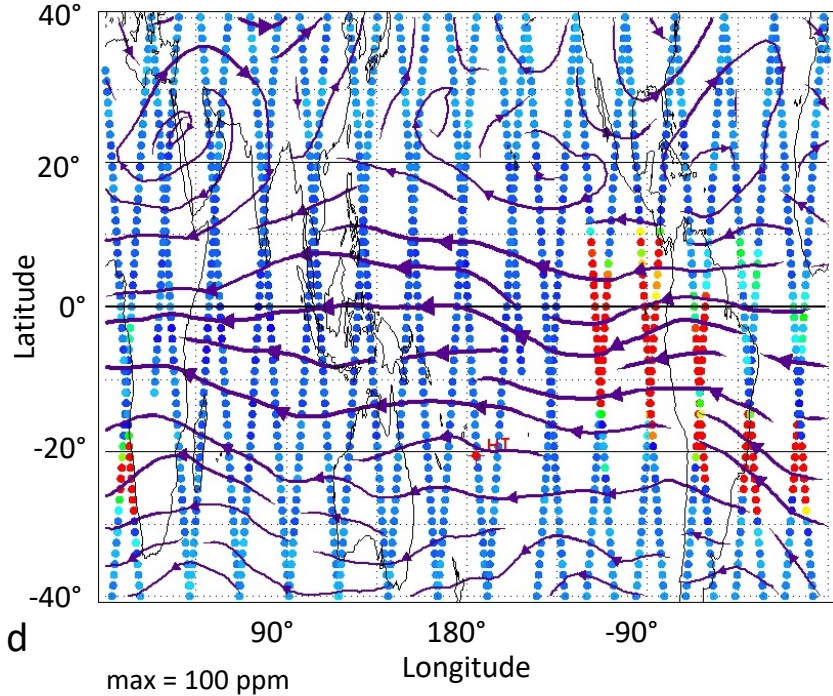
90° 180° -90°
Longitude

90° 180° -90°
Longitude

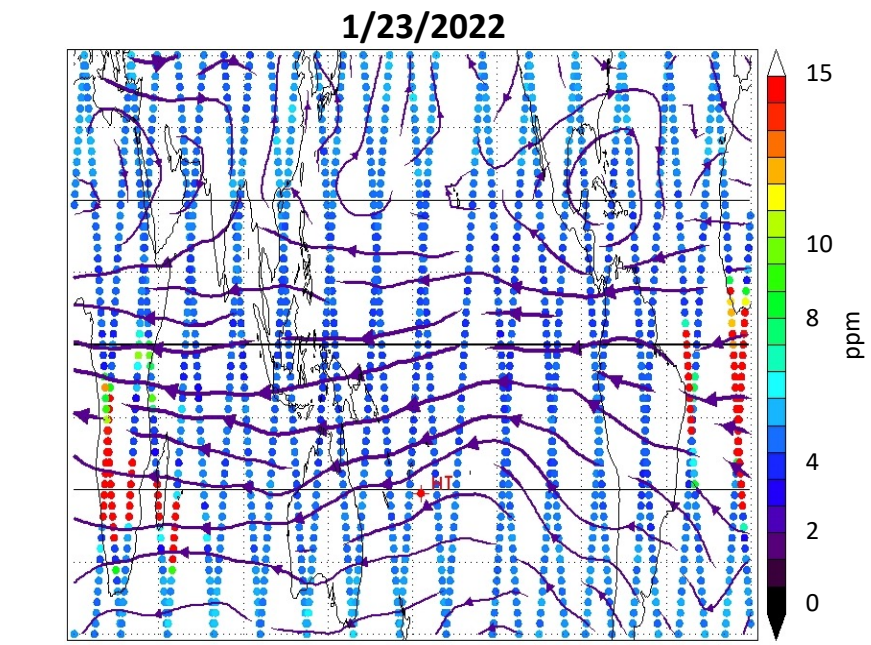
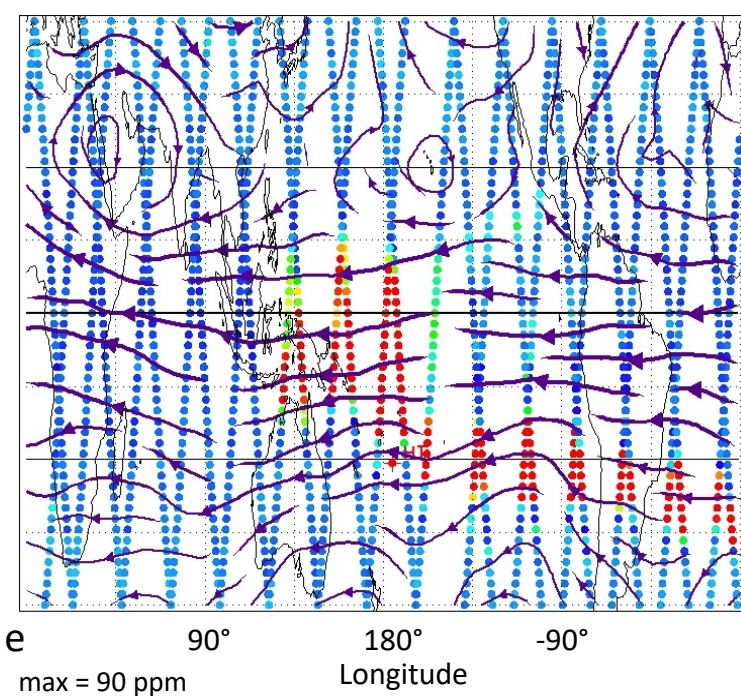
Figure 3.



a **1/26/2022**



b **1/30/2022**



c **2/15/2022**

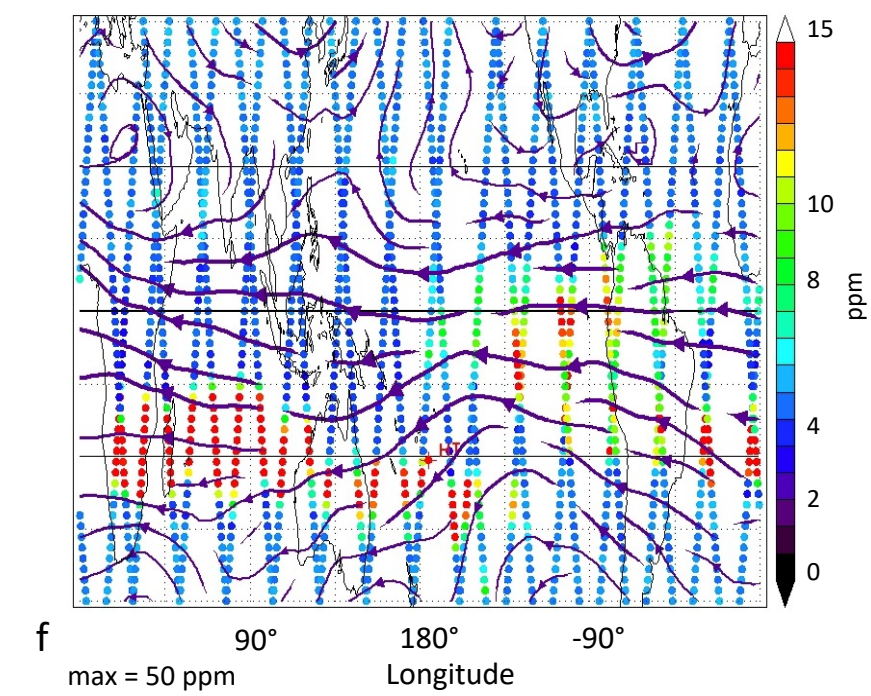
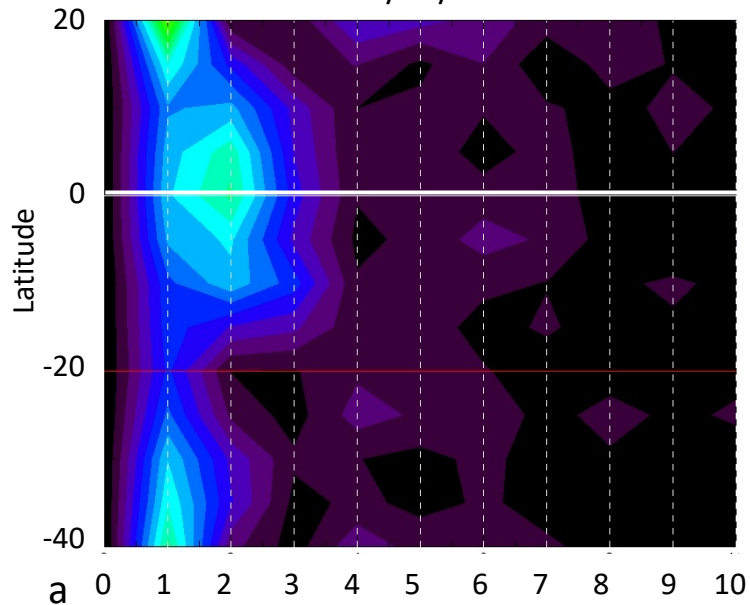
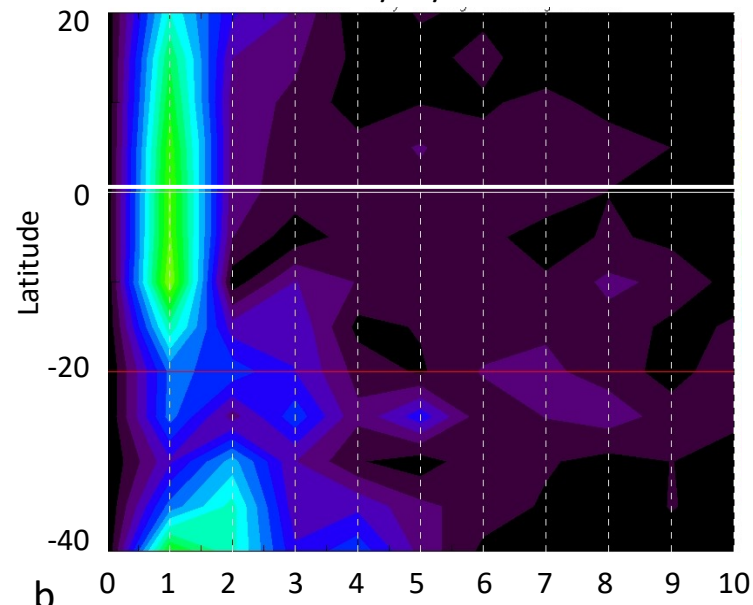


Figure 4.

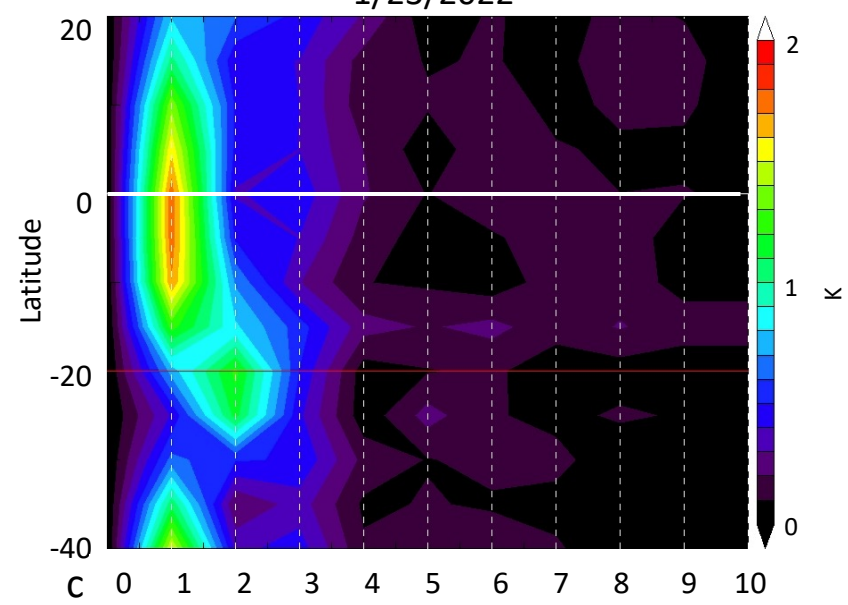
1/13/2022



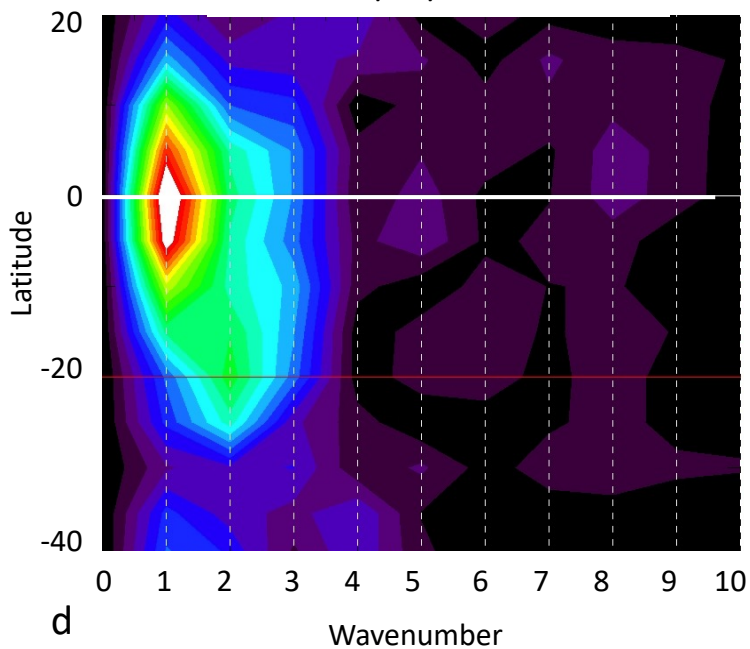
1/20/2022



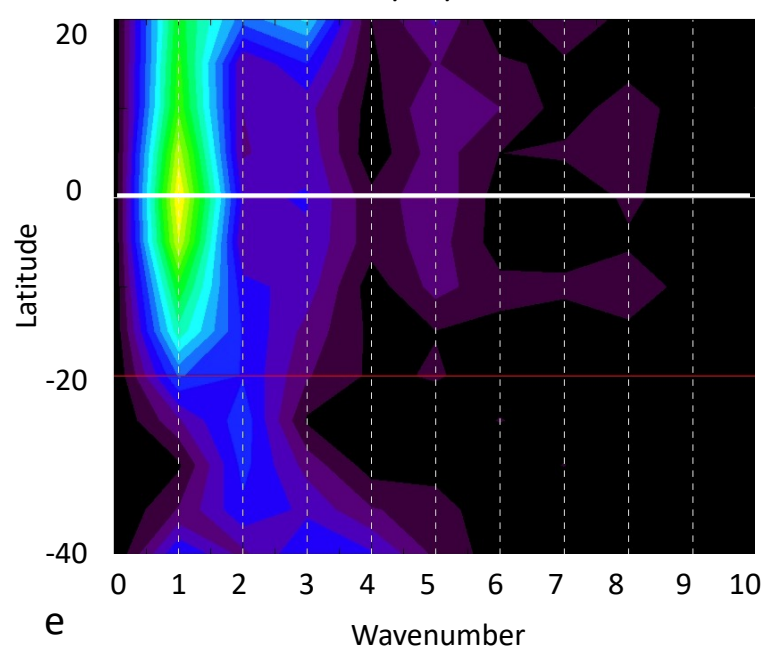
1/23/2022



1/26/2022



1/30/2022



5/1/2022

